


Implantable Multi-Modality Probe for Subdural Simultaneous Measurement of Electrophysiology, Hemodynamics, and Temperature Distribution

Toshitaka Yamakawa , *Member, IEEE*, Takao Inoue, Masatsugu Niwayama, *Member, IEEE*, Fumiaki Oka, Hirochika Imoto, Sadahiro Nomura, and Michiyasu Suzuki

Abstract—Objective: The purpose of this paper is to demonstrate how the integration of the multi-channel measurement capabilities of near-infrared spectroscopy (NIRS), electrocorticography (ECoG), and negative temperature coefficient thermistor sensors into a single device compact enough for subdural implantation can provide beneficial information on various aspects of brain cortical activity and prove a powerful medical modality for pre-, intra-, and post-operative diagnoses in neurosurgery. **Methods:** The development of a flexible multi-modal multi-channel probe for the simultaneous measurement of the NIRS, ECoG, and surficial temperature obtained from the cerebral cortex was carried out. Photoelectric bare chips for NIRS channels, miniature temperature-coefficient thermistors for measuring localized temperature variation, and 3-mm-diameter platinum plates for ECoG recording were assembled on a polyimide-based flexible printed circuit to create six channels for each modality. A conformal coating of Parylene-C was applied on all the channels except the ECoG to make the probe surface biocompatible. **Results:** As a first-in-human study, the simultaneous measurement capability of the multi-modality probe, with sufficient signal-to-noise ratio and accuracy, to observe pathological neural activities in subjects during surgery and post-operative monitoring, with no complications two weeks since the implantation, was confirmed. **Conclusion:** The feasibility of using a single device to assess the dynamic pathological activity from three different aspects was determined for human patients. **Significance:** The simultaneous and accurate multi-channel recording of electrical, hemodynamic, and thermographic cortical activities in a single device small enough for subdural implan-

tation is likely to have major implications in neurosurgery and neuroscience.

Index Terms—Near-infrared spectroscopy, electrocorticography, brain temperature, multi-modality probe, subdural implantation, flexible electronics.

I. INTRODUCTION

INVASIVE means for the measurement of cortical activity are widely used before, during, and after brain surgery since they provide information that outweigh negative effects such as the risk of infection. Electrocorticogram (ECoG), which measures electrical activity directly from the cerebral cortex using cortical surface grids or intracerebral electrodes, is fundamental to the pre-surgical evaluation of epilepsy [1], [2]. Several studies have found non-invasive methods for the simultaneous recording of electroencephalogram (EEG) and near-infrared spectroscopy (NIRS) data to detect reliable clinical indicators for the evaluation of epilepsy [3], [4]. However, studies have found that invasive and direct cortical measurement methods provided more meticulous information on the interaction between electrical and hemodynamic activities, due to higher signal-to-noise (S/N) ratio and finer spatial resolution [5]–[7]. Thus, the integration of multi-modality capability with a single, less invasive, and miniaturized measurement procedure could provide strict spatio-temporal concordance between results from multiple diagnostic aspects.

In a previous study, we had developed a polyimide-based flexible NIRS-ECoG sensor with a miniaturized probe that enabled chronic subdural implantation. A fabrication process based on semiconductor manufacturing technology achieved the integration of four ECoG electrodes and an NIRS channel within a 5.6×10 -mm probe-head with a total thickness of 0.7 mm. The prototype probe had achieved the simultaneous measurement of ECoG and NIRS data of a rat brain during craniotomy [8].

In this paper, the measurement of surficial cortical temperature is carried out, and enhanced, using negative temperature coefficient (NTC) thermistors, and the probe shape and channel spacing for rat brain specimens are redesigned to match those of human cerebral cortex in reference to subdural strip electrode, which is a standard device for invasive ECoG measurement.

Manuscript received November 21, 2018; revised February 17, 2019; accepted February 25, 2019. Date of publication February 28, 2019; date of current version October 18, 2019. This work was supported in part by JSPS KAKENHI under Grants 15H05356 and 15H05719, and in part by AMED-SENTAN under Grant 17934809. (Corresponding author: Toshitaka Yamakawa.)

T. Yamakawa is with the Division of Informatics and Energy, Faculty of Advanced Science and Technology, Kumamoto University, Kumamoto 860-8555, Japan, and also with the Fuzzy Logic Systems Institute, Iizuka 820-0067, Japan (e-mail: yamakawa@cs.kumamoto-u.ac.jp).

T. Inoue, F. Oka, H. Imoto, S. Nomura, and M. Suzuki are with the Department of Neurosurgery, Graduate School of Medicine, Yamaguchi University.

M. Niwayama is with the Research Institute of Electronics, Shizuoka University.

Digital Object Identifier 10.1109/TBME.2019.2902189

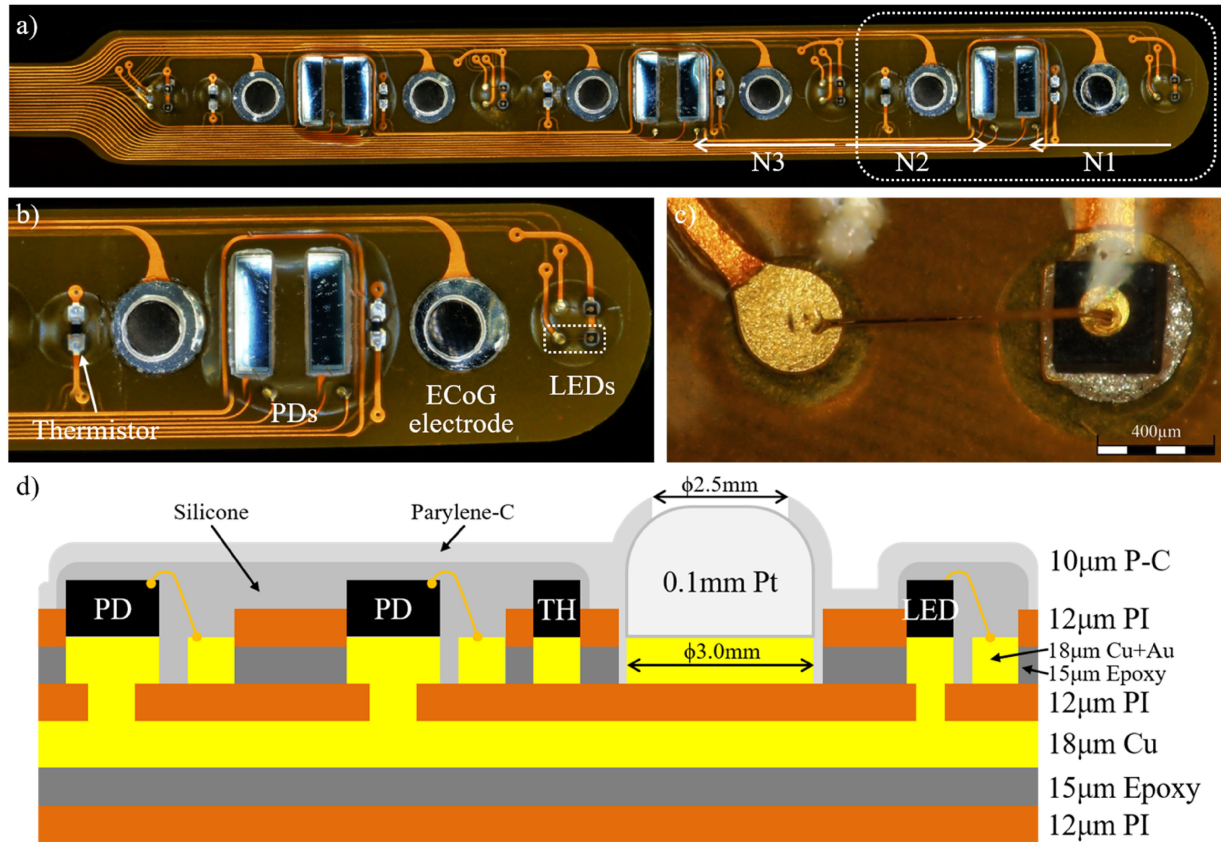


Fig. 1. Microscopic photographs of the fabricated probe. (a) Overall view of the probe-head showing six ECoG, temperature, and NIRS channels. N1-N3 and white arrows are examples of NIRS measurement regions realized by time-sharing of LEDs and PDs. (b) Magnified view of the white dotted area in (a). The gold and dark patterns show the conductive patterns of top and bottom layers, respectively. The circular patterns on the platinum ECoG electrodes are the edges of the removed Parylene-C coating. (c) Magnified view of the white dotted area in (b) showing the aperture holes of the coverlay, the bonding pads, and the wire-bonded LED sealed in water-clear silicone. The top and bottom of the LED are connected by a gold bonding wire and silver paste to the pads. (d) A schematic cross-sectional image of the probe. The materials and layer thicknesses are shown in the right edge. Polyimide and Parylene-C are abbreviated as PI and P-C in the schematic, respectively.

The probe structure, conformation of sensor components, fabrication method, and measured physiological indices are discussed in Section II. The experimental methods and results are detailed in Sections III and IV, respectively. Section V discusses the results obtained from an instrumentation and biomedical engineering standpoint. The concluding remarks and the future works are summarized in Section VI.

II. MATERIALS AND METHODS

A. Probe Fabrication

In order to achieve a fine conductive pattern to realize a multi-channel multi-modal sensing capability suitable for a small cortical region, a thickness compatible with subdural implantation, and a mass-production capability suitable for disposable usage, flexible printed circuit technology was used to fabricate the proposed probe. Two conductive copper layers of a polyimide substrate were processed by photolithography to form wiring patterns and bonding pads, and ECoG electrodes with vertical connection plated through holes between the layers. Both the layers were given a finishing using electroless gold plating to prevent toxicity and improve biocompatibility. Both the conductive lay-

ers, except for the ECoG electrodes and bonding-pad layers, were laminated with polyimide coverlays on the inner surface using vacuum heating press. A total substrate thickness of approximately 75 μm can achieve flexibility sufficient for cortical measurement.

The probe head was designed to have an outer shape similar to that of the subdural strip electrodes commonly used in neurosurgery. Six Au-plated, 3-mm-diameter circular patterns of the ECoG electrodes are aligned with a 1-cm spacing on an 8-mm-wide rounded-edge substrate strip as shown in Fig. 1(a). A 0.1-mm-thick platinum plate was processed via die-cutting press to obtain a convex dome of 0.4-mm height and 3-mm diameter. The fabricated platinum dome was then mounted on the Au-plated circular patterns by re-flow soldering. These six convex platinum electrodes were used for ECoG recording for compatibility with subdural chronic implantation.

The measurement channel of NIRS was fabricated by using a pair of infrared LED bare chips having different wavelengths (C770-40P for 770 nm, C810-40P for 810 nm, 0.4 × 0.4 × 0.25 mm, Epitex, Kyoto, Japan) and a photodiode (PD) bare chip (PD2501, 1.3 × 3.1 × 0.3 mm, Epitex). The LEDs and photodiodes are mounted on either side of the ECoG

electrode to establish an appropriate source-detector distance for measuring the same cortical region as the electrode, as shown in Fig. 1(b). The top and bottom electrodes of the bare chips were connected to the bonding pads using 25- μm -diameter gold bonding wires and conductive silver paste, respectively.

Negative-temperature-coefficient thermistors (ERTJZEG-103FA, 10 k Ω at 25 $^{\circ}\text{C}$, $0.6 \times 0.3 \times 0.3$ mm, Panasonic, Osaka, Japan) were used to measure the surficial temperature of the cerebral cortex. The thermistors were soldered on the pair of bonding pads assembled in close proximity to the ECoG electrode.

After assembling the circuit, all electronic components including bonding wires and pads were sealed with non-toxic, water-clear silicone. Subsequently, all components and the substrate were coated with a 10- μm -thick Parylene-C layer for insulation biocompatible with chronic implantation. The Parylene-C layer around the center (diameter = 2.5 mm) of ECoG electrodes was mechanically removed to expose the platinum electrode surface, as shown in Fig. 1(d). Therefore, the acute toxicity of the fabricated probe was eliminated from all the materials exposed to the cortical surface. The maximum total thickness of the probe-head after the assembly was found to be approximately 0.7 mm.

The recording channels are numbered from right to left in Fig. 1(a), denoted by the initial letter of the recording modality, e.g., the ECoG electrode at the probe tip is E1, the third NIRS channel from the probe tip is N3, and the thermistor output located near the probe's root is T6.

B. Hemoglobin Concentrations From NIRS

The LEDs ran on an applied power of 1 mW in the following sequence: The 770-nm LED for N1 [defined in Fig. 1(a)] was turned on for 20 ms, followed by a resting period of another 20 ms; the 810-nm LED for N1 was turned on for 20 ms; the LED pair for N2 was then turned on/off repeatedly; and, after the 240 ms on the on/off sequence of the six NIRS channels, all the LEDs were turned off for a static period of 260 ms.

The photoelectric current obtained by the PD was processed using a current-to-voltage converter and an amplifier on a custom circuit board whose channels were multiplied from [8] and fed into a personal computer via a digitizer. The mean voltages of the luminous period and static period triggered by the LED driving signals were used for the following calculation:

The changes in oxyhemoglobin, deoxyhemoglobin, and total hemoglobin concentrations were obtained as shown in [9]:

$$\Delta [\text{HbO}_2] = \frac{7.8679 \Delta OD_{810} - 4.4153 \Delta OD_{770}}{l}, \quad (1)$$

$$\Delta [\text{HHb}] = \frac{5.1373 \Delta OD_{810} - 3.7166 \Delta OD_{770}}{l}, \quad (2)$$

$$\Delta [\text{HbT}] = \Delta [\text{HbO}_2] + \Delta [\text{HHb}]. \quad (3)$$

ΔOD is optical density expressed as $\ln(I_0/I)$, where I and I_0 are the measured and initial optical intensities, respectively, at each wavelength, and the coefficients of ΔOD were calculated from the molecular extinction coefficient at each wavelength

[10]. In this paper, the instantaneous optical intensity at $t = 0$ was used for the value of I_0 in each experiment. l is the mean optical path length obtained by the Monte Carlo simulation [11]. A homogeneous model was used for the simulation on the assumption that the probe measured directly the cortical surface without any reflected and scattered layers. The Monte Carlo simulation was performed with the following optical parameters: an absorption coefficient, μ_a , of 0.04 mm^{-1} and a scattering coefficient, μ_s , of 42 mm^{-1} , assuming the gray matter of the cortical surface [12], and an anisotropy factor, g , of 0.95 under the consideration of forward scattering in the homogeneous model [13]. As a result of the simulation, the value $l = 37.4$ mm was derived for the PD at 8 mm from the LEDs [14].

C. Temperature Compensation

The cortical surface temperature was obtained from the thermistor resistance monitored by a thermal signal conditioner (M3SXR-7V-R, M-System Co., Ltd., Osaka, Japan). The signal conditioner drove the thermistors in parallel with 10 V_{DC} while monitoring the thermistor resistance, and it was programmed to give a linear output in the range of 0–10 V for a temperature in the range of 0–45 $^{\circ}\text{C}$ using the temperature-resistance table of the thermistor with a time constant of 0.1 second. A portable temperature calibrator (KT-H504, CHINO, Tokyo, Japan) was used to calibrate the properties of the built-in thermistor of the multimodality probe. The multimodality probe (calibration target) and a reference thermometer (USB Reference Thermometer, ThermoWorks, Salt Lake City, USA) were inserted into the two insertion holes of the metal block in the calibrator made of a high-thermal-conductivity material. To collect the temperature recorded by the multimodality probe, the metal block temperature was varied in steps of 5 $^{\circ}\text{C}$ (5–10 min per step) in the range of 0–50 $^{\circ}\text{C}$ on the basis of the reference thermometer. Finally, a calibration curve correlating temperatures recorded by the multimodality probe and the reference thermometer was established, and the temperature-resistance table was updated to fall within the range of ± 0.1 $^{\circ}\text{C}$. The thermal voltage (V_T) signals were collected by a digitizer and fed into a computer simultaneously with the NIRS and ECoG signals, and the values were transformed into Celsius temperature (θ) by the equation of $\theta = 4.5V_T$ in an offline post process.

III. EXPERIMENTAL METHODS

The experimental procedure was reviewed and approved by the Yamaguchi University Institutional Review Board, and it conformed to the Helsinki Declaration. The patients and their families agreed to participate in our study after being adequately informed of the aims, methods, and anticipated benefits, as well as the potential risks and discomfort associated with their involvement; all patients had the right to withdraw from the study at any time.

A. Data Acquisition

The ECoG electrodes were connected to an EEG amplifier (EBM-1016; Unique Medical Co., Ltd., Tokyo, Japan) with a

filter setting of DC–1000 Hz passband. The NIRS, pre-conditioned ECoG, and thermistor signals, and physiological activities (arterial blood pressure and electrocardiogram) monitored by a perioperative monitor were simultaneously collected at a sampling rate of 200 Hz and stored on a computer via two digitizers (AIO-163202FX-USB; Contec Co., Ltd., Osaka, Japan) and a controller software (LabDAQ5-CT Multi, Matsuyama Advance Co., Ltd., Ehime, Japan). In addition, the ECoG signals for broadband frequency analysis were collected in a 2-kHz sampling frequency by a physiological data acquisition device (PowerLab 8/35; AD Instruments, Colorado Springs, USA) in parallel with the Contec digitizers. Changes in oxy-hemoglobin, deoxyhemoglobin, and total hemoglobin concentrations were calculated offline by the methods described in Section II.

B. Experimental Procedure

The multi-modal measurement function of the fabricated probe in two clinical subjects was examined. During this examination, in advance of the clinical experiment, the toxic and foreign-body responses under long-term implantation in experimental animal subjects (rodents, felines, and macaques) were studied. The safety and efficacy of the fabricated device along with the experimental protocols were approved by the research ethics committee. A detailed explanation of the measurement capability required for chronic implantation, however, will be studied in a future research paper under preparation.

1) Intraoperative Monitoring: Focal brain cooling suppresses epileptic discharges with minimal impact on neurological functions [15]. In our previous research [8], the simultaneous recording of NIRS and ECoG in a rat subject revealed the hemodynamic response during focal brain cooling. In the present experiment, the fabricated probe was used to observe the response of the epileptic focus to focal brain cooling during epilepsy surgery. The subject with intractable extra-temporal lobe epilepsy was anesthetized with 2.5% sevoflurane on complaints of irritation to enhance interictal epileptiform discharges.

The fabricated device sterilized by EOG was placed in the cortical region of the planned resection area, which was preliminarily determined by pre-surgical evaluation. The probe-head was covered by a thin, transparent drape to attain fixation and tight contact between the probe and the cortical surface, and a part of the probe was enshrouded by a square-shaped Ti cooling device (30 mm × 30 mm). Finally, the ECoG channels E3–6 of the fabricated probe were placed beneath the cooling device, and E1 and E2 were inserted into the subdural cavity from the edge of the cranial window as shown in Fig. 2.

2) Postoperative Monitoring: A patient of aneurysmal subarachnoid hemorrhage (SAH) in Yamaguchi University Hospital Advanced Medical Emergency and Critical Care Center was selected to undergo post-operative monitoring using the newly developed probe, in compliance to standard protocol. Clipping surgery with simultaneous decompressive craniotomy allowed the placement of the multi-modality probe on the ipsilateral frontal lobe surface through a cranial window as shown in Fig. 3. The SAH was diagnosed using contrast-enhanced computed tomography (CT) scan.

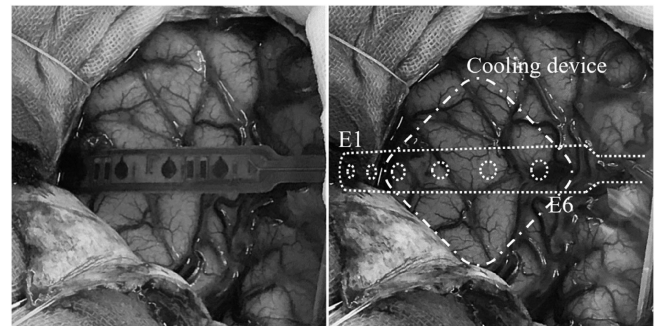


Fig. 2. Photographs of the cranial window during and after measurement using the fabricated probe. The location of the fabricated probe and the cooling device are illustrated with the dot and dot-dashed lines, respectively (right).

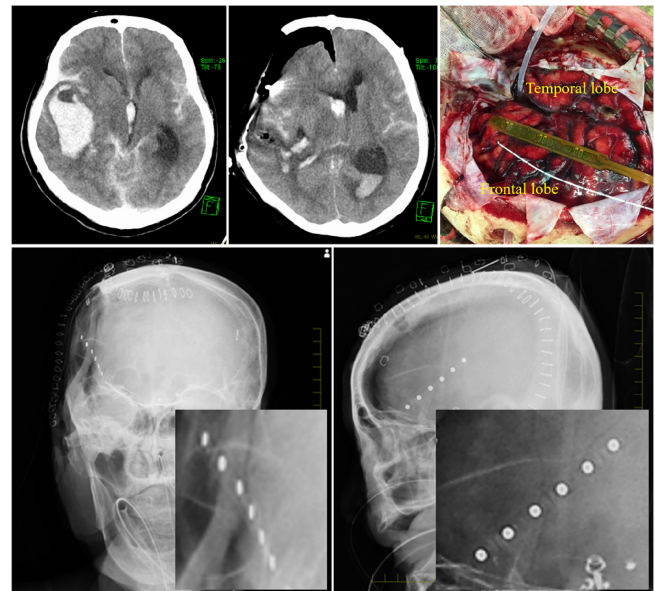


Fig. 3. X-ray images of before and after clipping surgery (upper left and middle), and the proposed probe in postoperative monitoring (lower). A picture of the surgery (upper right) shows that the bright red color of the cortical surface was significantly different from that of healthy brain because the region was affected by SAH. The platinum electrodes mounted on the probe appear similar to strip electrodes and the light shadows of the mounted PDs are visible in the magnified view (lower right).

We placed the multi-modality probe on the cortical surface of the vascular territory of the aneurysm-carrying vessel in patients who underwent neck clipping and decompressive craniotomy as mentioned previously [16]. The recording was performed following the recently published recommendations of the cooperative studies on brain injury depolarizations [17].

IV. EXPERIMENTAL RESULTS

A. Response to Intraoperative Focal Brain Cooling

Fig. 4 shows the channels recorded during focal brain cooling, where the cooling period starts at $t = 0$ min and ends at $t = 10$ min. A sectional temperature degradation manifested on the recording channels T4 and T5 in accordance with the cooling section. Temperature degradation in T2, T3, and T6, which are located in proximity to the cooling area, responds slower

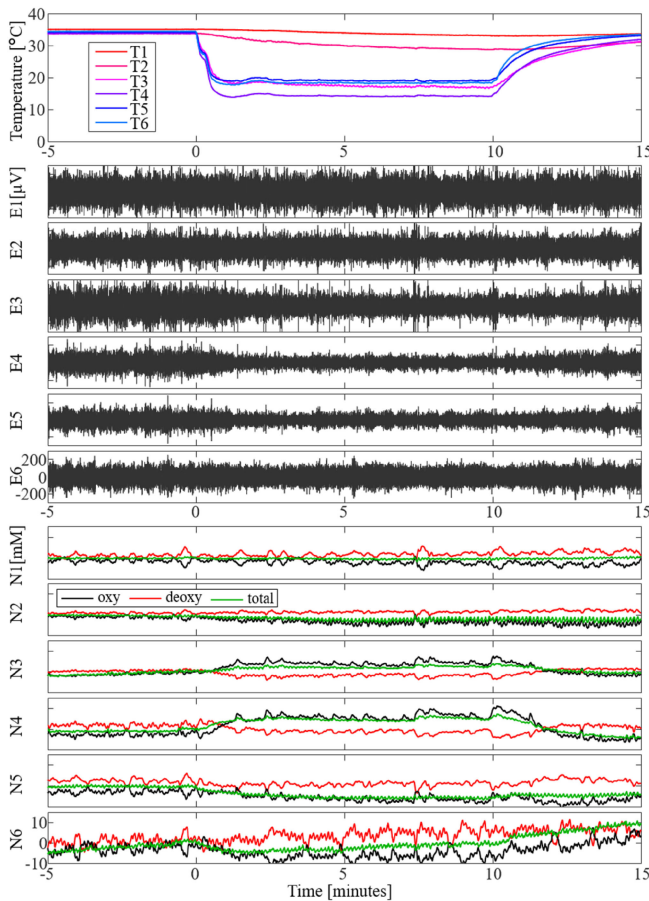


Fig. 4. Simultaneously recorded multi-channel multi-modality signals during focal brain cooling where cooling starts at $t = 0$. The vertical scale for each modality is unified. In the NIRS traces, $\Delta[\text{HbO}_2]$, $\Delta[\text{HHb}]$, and $\Delta[\text{HbT}]$ are represented with black, red, and green lines, respectively.

when compared to T4 and T5. Thermistor T1 did not show any significant temperature change.

The amplitude of the ECoG channels, especially those of E4 and E5, dampened during the cooling phase and gradually recovered as the cortical temperature was increased.

In the NIRS channels N3 and N4, which are located below the cooling device, the O_2Hb and HbT levels increased slightly after the start of the cooling phase. The baseline fluctuation was within $50 \mu\text{M}$, which is estimated to be due to the respiratory artifacts that appeared in O_2Hb and HHb levels. Despite T5 and T6 demonstrating sufficient cooling, channels N5 and N6 did not indicate any hemoglobin change related to the cooling.

B. Neuropathological Activity in Postoperative Monitoring

As shown in Fig. 5, the multimodal signals during a 35-min interval, when the neuropathological activity was observed, are extracted from 14 days of recording. The calculated hemoglobin concentrations and temperature signals smoothed with the moving average of a 10-sec time window to eliminate the change due to artifacts occurring during processes such as respiration and pulsation. The trends in the top box show the DC component of ECoG electrode extracted by a software band-pass filter with the passband of DC–1.0 Hz to highlight the transition of

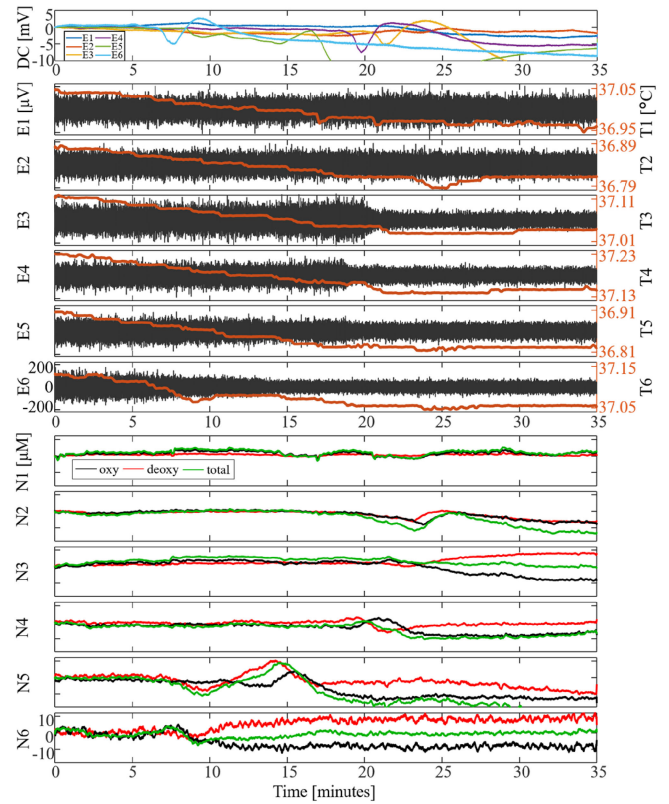


Fig. 5. Simultaneously recorded multi-channel multi-modality signals in post-operative monitoring. The vertical scale for each modality is unified.

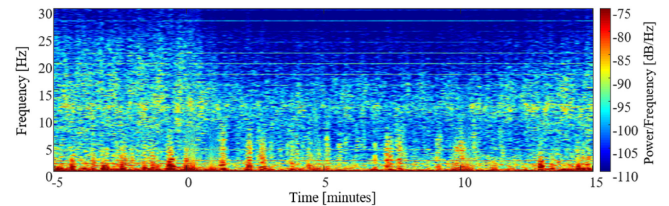


Fig. 6. A spectrogram of E4 in the monitoring of focal brain cooling. A significant power reduction with temperature degradation in T4 was observed.

cortical spreading depolarization (CSD). CSD is a pathological phenomenon characterized by a region of hyperactivity followed by a region of suppressed electrical activity, from where the depressed region propagates at a velocity of 2–3 mm/minute [18], and can be observed by negative DC shift in ECoG. Since the depressed region propagated from E6 to E3 within a time period of 7 to 21 minutes, this change was found to be due to CSD.

The gradual temperature degradation observed in all the thermistors used in this experiment until the onset of CSD was accompanied by body temperature degradation, which was confirmed by simultaneously measured bladder temperature.

V. DISCUSSION

The ECoG amplitude in the cooling region dampened along with the degradation in cortical temperature as shown in Fig. 4. In the spectrogram of E4 shown in Fig. 6, a significant power

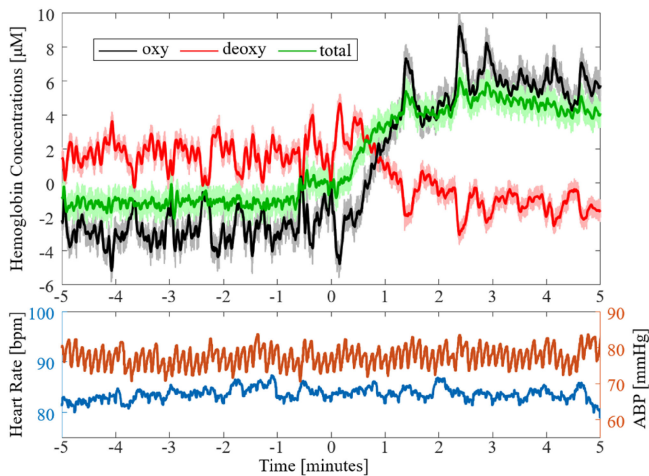


Fig. 7. The NIRS signals in N4 (upper), the heart rate, and arbitrary blood pressure traces (lower).

reduction was observed in a frequency range higher than 15 Hz, which is consistent with the results of our previous study [19].

The dilution of oxyhemoglobin concentration during focal brain cooling in the NIRS channels N3 and N4 implies the deceleration of oxygen metabolism in the cooling region. The enlarged view of N4 at $t = -5$ –5 min are shown in the upper traces in Fig. 7 where the brighter and darker curves are before and after the smoothing of two-second moving average. The lower box of Fig. 7 shows the changes in heart rate and arterial blood pressure simultaneously collected by the anesthesia monitor. Since it is synchronized with the blood pressure fluctuation, the baseline fluctuation with an amplitude of 1–2 μM and frequency of approximately 0.15 Hz is a reflection of the respirative artifacts. This synchronization of respirative Hb with the blood pressure fluctuation explains why, in this case, the frequency of fluctuation was observed to be independent of heart rate and instead a result of respirative artifacts.

Despite adequate temperature reduction in T5 and T6, no significant change in hemoglobin level due to the cooling was observed in the NIRS channels N5 and N6 in Fig. 4. This is plausibly due to that the PDs used in N5 and N6 located on a blood vessel as shown in Fig. 2, because the NIR light is almost completely absorbed by the blood vessels larger than 1-mm diameter [20], [21].

In our previous report, we had inserted NIRS sensors of identical specifications onto the cortical surface of anesthetized rats and performed focal brain cooling, which resulted in a slight increase in the O_2Hb level and a strong reduction in the HHb level. In contrast, in the present results, the O_2Hb level and HHb level showed a sharp increase and an insignificant decline, respectively. This difference may be related to the epileptic foci of the cooling site in human cerebral cortex. Epileptic foci have a condition similar to ischemia (high HHb, low O_2Hb) due to the occurrence of interictal epileptic activity even when the demand for blood flow is stable. Since focal cooling is known to improve ischemic state [22] the O_2Hb level in the human cerebral cortex, unlike those in healthy rat brains, is found to increase strongly. Accordingly, the HHb level was slightly hindered due

to the relatively small blood volume. Studies confirm a correlation between total Hb level and cerebral blood flow rate [23], [24]. In contrast, the results detailed in this section reveal an increase in cerebral blood flow after the cooling. However, it should be noted that cooling slows down cerebral blood flow and does not increase it. Therefore, the indirect evaluation of cerebral blood flow during monitoring by NIRS requires comprehensive evaluation of the change in total Hb level as well as calculation of tissue oxygen saturation and low-frequency vascular fluctuations [25].

During post-operative monitoring, the fabricated sensor measured the spreading depolarization and depression. While the reduction in amplitude in ECoG was observed in the AC band, the distinct temperature changes associated with CSD were observed in the DC band.

Distinct temperature changes associated with CSD were observed in channels T2 and T6. In T6, the temporal temperature degradation in the 10-minute duration was observed a few minutes after the negative DC shift in ECoG and the CSD-like hemoglobin change in NIRS. Although a significant negative DC shift was not observed in E2, a hemoglobin change was observed in N2 followed by a similar temporal temperature change in T2. Despite cerebral temperature control being crucial in intensive-care situations, the clinical use of temperature sensors compatible with subdural implantation is uncommon. Recently, several studies have reported the temperature increase associated with CSD [26], [27]. The proposed multi-channel implantable thermistor, in principle, is feasible for such focally moving minimal temperature gradients. On the other hand, unlike in previous studies, the results in Fig. 5 show a temperature degradation of 0.02–0.03 $^\circ\text{C}$. Although more experiments considering intra- and inter-subject variance are required, the reversed change would demonstrate the latter half of the transient temperature elevation, since degradation appears slightly behind the occurrence of CSD. Furthermore, the variation is consistent with the temperature gradient described in the preceding reports. A study involving the use of a mathematical neuronal model for the evaluation of energy production in the cerebral cortex revealed that the temperature increase caused by CSD is in the 5–30 mK range [28]. Even though such fine temperature resolution was not achieved by the proposed device, it should be realized with the improvement of signal-to-noise ratio by inserting a built-in filter and grounded electromagnetic shield patterns, which can be easily modified on the measurement system and the substrate conductive pattern. The usage of a packaged high-resolution digital temperature sensor (e.g., LTC2983, Analog Devices, Norwood, USA) is also a promising solution to obtain a temperature resolution of tens of mK.

Several studies have reported that brain temperature varies according to the pathology of the epilepsy-inducing disease. Our previous study using a rat epilepsy model showed that penicillin-induced epileptiform discharges elevated the focal brain temperature; the mean increase was approximately 0.65 $^\circ\text{C}$ [29]. In addition, the recent development of non-invasive cerebral temperature recording using magnetic resonance imaging (MRI) indicated the focal hyperthermia related to epileptiform activity [30]. Therefore, we monitored the brain temperature gradient

in subjects who suffered from SAH to verify the performance of our sensor. Demonstrated in this paper, a temperature measurement capability with resolution finer than 0.1 °C is highly likely to provide beneficial clinical efficacy in detecting abnormal neuronal activity.

The NIRS signal's accurate response to CSD was shown to be due to an increase in deoxyhemoglobin level and decrease in oxyhemoglobin level, which coincides with the results obtained from a previous study we conducted on the NIRS signal response to hypoxic brain conditions in a rat subject. Since such changes were found to be associated with CSD in a hypoxic brain [31], the results obtained suggest that the changes in hemoglobin levels were caused by pathologically induced CSD after SAH. On the other hand, in the study that showed instantaneous response of NIRS to CSD, biphasic patterns were observed in both oxy- and deoxy-hemoglobin concentrations. Although further discussions with a larger sample group of subjects are needed to understand the full effect and applications, the proposed probe has proven advantageous in developing measurement capability to achieve such instantaneous responses, which have not been reported by other studies in the field.

Since biomedical implantable devices must be single-use and disposable, flexible printed circuit technology, used in the fabrication of the proposed probe, makes mass production at low cost feasibility. The processes of re-flow soldering and wire bonding used for parts assembly were operated in a machine process. Furthermore, vacuum vapor deposition for Parylene-C coating can also be automated, although thermal etching of the Parylene-C insulator above the platinum electrodes may require manual procedure. Therefore, the proposed probe can provide critical information on multi-modal neuronal activity at lower price-per-channel when compared to the conventional ECoG strip or grid electrodes, which are mostly developed by manual fabrication process.

VI. CONCLUSION

This research paper introduced a compact and flexible multi-modal probe for simultaneous multi-channel recording of NIRS, ECoG, and temperature distribution. The device was fabricated and assembled using flexible printed circuit technology and semiconductor microfabrication technology for high-density integration of sensor components compatible with subdural implantation, and has a compact profile similar to that of the subdural strip electrodes commonly used in neurosurgery. The experimental results achieved through focal brain cooling of the participating subjects with epilepsy during the neurosurgical treatment demonstrated the desired electrical and hemodynamic activity, which were modulated by lowering the temperature. In the clinical study with post-operative SAH patients, the fabricated probe collected data on the dynamics and locational transition of the spontaneous pathological activity with ECoG suppression, transient change in the hemoglobin concentrations, and temperature gradient less than 0.1 K under two weeks after subdural implantation without any complications. Although there is a need to conduct further studies with larger subject sample size and trials to prove clinical efficacy, the results of the

present study have demonstrated the feasibility of assessing the dynamic pathological activity from three different modalities in a single apparatus with minimal surgical invasion.

REFERENCES

- [1] G. Alarcon, "Origin and propagation of interictal discharges in the acute electrocorticogram implications for pathophysiology and surgical treatment of temporal lobe epilepsy," *Brain*, vol. 120, no. 12, pp. 2259–2282, Dec. 1997.
- [2] A. Hufnagel *et al.*, "Clinical relevance of quantified intracranial interictal spike activity in presurgical evaluation of epilepsy," *Epilepsia*, vol. 41, no. 4, pp. 467–478, Apr. 2000.
- [3] N. Roche-Labarbe *et al.*, "NIRS-measured oxy- and deoxyhemoglobin changes associated with EEG spike-and-wave discharges in children," *Epilepsia*, vol. 49, no. 11, pp. 1871–1880, Nov. 2008.
- [4] A. Machado *et al.*, "Detection of hemodynamic responses to epileptic activity using simultaneous electro-encephalography (EEG)/near-infrared spectroscopy (NIRS) acquisitions," *Neuroimage*, vol. 56, no. 1, pp. 114–125, May 2011.
- [5] V. Osharina *et al.*, "Local haemodynamic changes preceding interictal spikes: A simultaneous electrocorticography (ECoG) and near-infrared spectroscopy (NIRS) analysis in rats," *Neuroimage*, vol. 50, no. 2, pp. 600–607, Apr. 2010.
- [6] Y. Sato *et al.*, "Hemodynamic and electrophysiological connectivity in the language system: Simultaneous near-infrared spectroscopy and electrocorticography recordings during cortical stimulation," *Brain Lang.*, vol. 123, no. 1, pp. 64–67, Oct. 2012.
- [7] M. Uga *et al.*, "Direct cortical hemodynamic mapping of somatotopy of pig nostril sensation by functional near-infrared cortical imaging (fNCI)," *Neuroimage*, vol. 91, pp. 138–45, May 2014.
- [8] T. Yamakawa *et al.*, "Development of an implantable flexible probe for simultaneous near-infrared spectroscopy and electrocorticography," *IEEE Trans. Biomed. Eng.*, vol. 61, no. 2, pp. 388–395, Feb. 2014.
- [9] M. Niwayama *et al.*, "Quantitative measurement of muscle hemoglobin oxygenation using near-infrared spectroscopy with correction for the influence of a subcutaneous fat layer," *Rev. Sci. Instrum.*, vol. 71, no. 12, pp. 4571–4575, Sep. 2000.
- [10] S. J. Matcher *et al.*, "Performance comparison of several published tissue near-infrared spectroscopy algorithms," *Anal. Biochem.*, vol. 227, no. 1, pp. 54–68, May 1995.
- [11] M. Niwayama *et al.*, "Error factors in oxygenation measurement using continuous wave and spatially resolved near-infrared spectroscopy," *J. Jpn. Coll. Angiol.*, vol. 52, pp. 211–215, Apr. 2012.
- [12] P. van der Zee *et al.*, "Optical properties of brain tissue," *Proc. SPIE*, vol. 1888, pp. 454–465, 1993.
- [13] W. F. Cheong *et al.*, "A review of the optical properties of biological tissues," *IEEE J. Quantum Electron.*, vol. 26, no. 12, pp. 2166–2185, Dec. 1990.
- [14] M. Niwayama and T. Yamakawa, "Implantable thin NIRS probe design and sensitivity distribution analysis," *Electron. Lett.*, vol. 50, no. 5, pp. 346–348, Feb. 2014.
- [15] M. Fujii *et al.*, "Cooling of the epileptic focus suppresses seizures with minimal influence on neurologic functions," *Epilepsia*, vol. 53, no. 3, pp. 485–493, Mar. 2012.
- [16] M. Fabricius *et al.*, "Cortical spreading depression and peri-infarct depolarization in acutely injured human cerebral cortex," *Brain*, vol. 129, no. Pt. 3, pp. 778–790, Mar. 2006.
- [17] J. P. Dreier *et al.*, "Recording, analysis, and interpretation of spreading depolarizations in neurointensive care: Review and recommendations of the COSBID research group," *J. Cereb. Blood Flow Metab.*, vol. 37, no. 5, pp. 1595–1625, May 2017.
- [18] C. Ayata and M. Lauritzen, "Spreading depression, spreading depolarizations, and the cerebral vasculature," *Physiol. Rev.*, vol. 95, no. 3, pp. 953–993, Jul. 2015.
- [19] H. Kida *et al.*, "Focal brain cooling terminates the faster frequency components of epileptic discharges induced by penicillin G in anesthetized rats," *Clin. Neurophysiol.*, vol. 123, no. 9, pp. 1708–1713, Sep. 2012.
- [20] H. Liu *et al.*, "Influence of blood vessels on the measurement of hemoglobin oxygenation as determined by time-resolved reflectance spectroscopy," *Med. Phys.*, vol. 22, no. 8, pp. 1209–1217, Aug. 1995.
- [21] T. J. Huppert *et al.*, "A temporal comparison of BOLD, ASL, and NIRS hemodynamic responses to motor stimuli in adult humans," *Neuroimage*, vol. 29, no. 2, pp. 368–382, Jan. 2006.

- [22] S. Nomura *et al.*, "Changes in glutamate concentration, glucose metabolism, and cerebral blood flow during focal brain cooling of the epileptogenic cortex in humans," *Epilepsia*, vol. 55, no. 5, pp. 770–776, May 2014.
- [23] T. Wolf *et al.*, "Systemic nitric oxide synthase inhibition does not affect brain oxygenation during cortical spreading depression in rats: A non-invasive near-infrared spectroscopy and laser-Doppler flowmetry study," *J. Cereb. Blood Flow Metab.*, vol. 16, no. 6, pp. 1100–1107, Nov. 1996.
- [24] L.-F. Liu *et al.*, "Measurement of cerebral blood flow and oxygen saturation using laser Doppler flowmetry and near infrared spectroscopy in ischemic stroke rats," *J. Med. Biol. Eng.*, vol. 28, no. 2, pp. 101–105, Mar. 2008.
- [25] J. P. Dreier *et al.*, "Cortical spreading ischaemia is a novel process involved in ischaemic damage in patients with aneurysmal subarachnoid haemorrhage," *Brain*, vol. 132, no. Pt. 7, pp. 1866–1881, Jul. 2009.
- [26] C. Li *et al.*, "Regional temperature and quantitative cerebral blood flow responses to cortical spreading depolarization in the rat," *J. Cereb. Blood Flow Metab.*, vol. 37, no. 5, pp. 1634–1640, May 2017.
- [27] A. J. Schiefecker *et al.*, "Brain temperature but not core temperature increases during spreading depolarizations in patients with spontaneous intracerebral hemorrhage," *J. Cereb. Blood Flow Metab.*, vol. 38, no. 3, pp. 549–558, Mar. 2018.
- [28] J. P. Dreier *et al.*, "Is spreading depolarization characterized by an abrupt, massive release of Gibbs free energy from the human brain cortex?" *Neuroscientist*, vol. 19, no. 1, pp. 25–42, Feb. 2013.
- [29] T. Tokiwa *et al.*, "Penicillin-induced epileptiform activity elevates focal brain temperature in anesthetized rats," *Neurosci. Res.*, vol. 76, no. 4, pp. 257–260, Aug. 2013.
- [30] D. Sone *et al.*, "Noninvasive detection of focal brain hyperthermia related to continuous epileptic activities using proton MR spectroscopy," *Epilepsy Res.*, vol. 138, pp. 1–4, Dec. 2017.
- [31] M. Seule *et al.*, "The hemodynamic response of spreading depolarization observed by near infrared spectroscopy after aneurysmal subarachnoid hemorrhage," *Neurocrit. Care*, vol. 23, no. 1, pp. 108–112, Aug. 2015.